Freezing Atoms in Motion: Principles of Femtochemistry and Demonstration by Laser Stroboscopy

J. Spencer Baskin and Ahmed H. Zewail*
Arthur Amos Noyes Laboratory of Chemical Physics, California Institute of Technology, Pasadena CA 91125

Freezing Atoms in Motion: Principles of Femtochemistry and Demonstration by Laser Stroboscopy

Outline

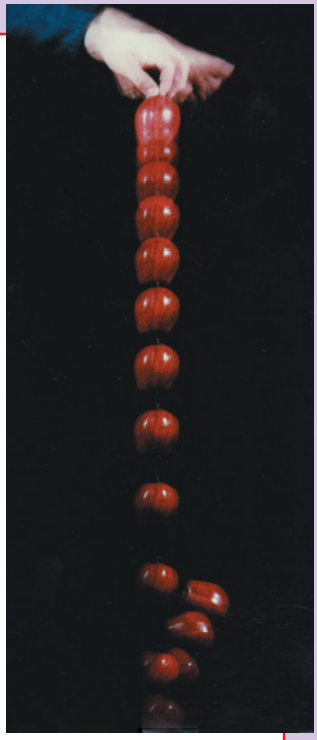

I. Introduction

The concept of the atom, proposed 24 centuries ago and rejected by Aristotle, was born on a purely philosophical basis, surely without anticipating some of the 20th century's most triumphant scientific discoveries. Atoms can now be seen, observed in motion, and manipulated (*1*). These discoveries have brought the microscopic world and its language into a new age, and they cover domains of length, time, and number. The *length* (spatial) resolution, down to the scale of atomic distance (angstrom, 1 Å = 10^{-8} cm), and the *time* resolution, down to the scale of atomic motion (femtosecond, 1 fs = 10^{-15} s), have been achieved. The trapping and spectroscopy of a single ion or electron and the trapping and cooling of neutral atoms have also been achieved. All these achievements have been recognized by the awarding of the Nobel Prize to scanning tunneling microscopy (1986), to single-electron and -ion trapping and spectroscopy (1989), to laser trapping and cooling (1997), and to laser femtochemistry (1999).

Before femtochemistry, the actual atomic motions involved in chemical reactions had never been observed in real time despite the rich history of chemistry over two millennia. Chemical bonds break, form, or geometrically change with awesome rapidity. Whether in isolation or in any other phase, this ultrafast transformation is a dynamic process involving displacements of electrons and atomic nuclei. The speed of atomic motion is ~1 km/s (10^5 cm/s), and hence, to record atomic-scale dynamics over a distance of an angstrom, the average time required is ~100 fs. The very act of atoms within molecules (reactants) rearranging themselves to form new molecules (products) is the focus of the field of femtochemistry. With femtosecond time resolution we can freeze atoms in motion and study the evolution of molecular structures as reactions unfold and pass through their transition states (configurations intermediate between reactants and products), giving a motion picture of the transformation.

Femtochemistry shares some common features with stop-motion photography using cameras with high-speed shutters and with flash stroboscopy, in which short light flashes illuminate an object under study. Capturing a well-defined image or impression of an object at a given point in its motion by short-duration illumination is the methodology common to all of these techniques. The technical requirements in each case are (i) attaining adequate spatial resolution to define the object of study and (ii) synchronization to a well-defined time-axis, permitting reconstruction of the dynamic process undergone.

This contribution discusses the basic principles of femtochemistry and the analogy to stop-motion photography. We describe an educational exhibit that highlights the experimental approach by demonstrating the use of light pulses in the study of a rapidly moving object. Some theoretical concepts unique to the molecular world of femtochemistry are discussed and illustrated with applications to real molecules.

II. Principles of Stop-Motion Photography

A. High-Speed Shutters

As a starting point, we may consider the historic experiments in stop-motion photography performed more than a hundred years ago by photographer Eadweard Muybridge. Some of those experiments, carried out under the patronage of Leland Stanford at Stanford's Palo Alto farm, are commemorated by a plaque on the campus of Stanford University (Fig. 1). Muybridge's work, which began in 1872, was inspired by a debate over the question of whether all four hooves of a trotting horse are simultaneously out of contact with the ground at any point in its stride. Muybridge believed he could answer this question by taking photographs with a camera shutter and film capable of capturing reasonably sharp images of a horse trotting at high speed. (The trot is a mode of locomotion, or gait, in which diagonal legs move together in pairs—it is a smooth, steady motion, in contrast to the more energetic bounding motion of the gallop, which is the gait used to attain ultimate speed for short distances. The details of each gait were eventually elucidated by Muybridge, but his written account clearly describes the seminal role of the trot in inciting his interest [*2*].)

We can estimate the duration of the shutter opening, Δt, that Muybridge needed for his camera from consideration of the necessary spatial resolution and the velocity υ of the horse. For a clearly defined image of a horse's legs, a resolution (Δx) of 1 cm is reasonable; that is, 1 cm is small compared to the relevant dimensions of the problem (the dimensions of the leg and its displacement during the course of a stride). Taking $\upsilon \approx 10$ m/s for the velocity of a horse (the legs will, in fact, at times be moving several times faster), and using the relation $\Delta x = \upsilon \Delta t$, leads to

$$\Delta t \approx \frac{1\ \text{cm}}{10\ \text{m/s}} = 10^{-3}\ \text{s} = 1\ \text{ms}$$

Indeed, Muybridge was able to achieve the necessary exposure times to capture an image of a trotting horse with all four feet in the air. Subsequent to this initial success, he devoted many years to the photographic study of animals and humans in motion, for some time in Palo Alto and later at the University of Pennsylvania (*2*).

Figure 1. Tablet erected on the Stanford University campus in 1929, commemorating "motion picture research" of Eadweard Muybridge at the Palo Alto farm of Leland Stanford in 1878 and 1879.

In these studies, Muybridge sought not only to provide the isolated images required to answer questions such as that which first attracted his interest, but also to document the entire sequence of an animal's leg motions during its stride. To establish the required absolute timing of the photographs, he initially set up a row of equally spaced cameras along a track at the Palo Alto farm. The shutter of each camera was activated by a thread stretched across the track in front of the camera. Thus a horse running down the track at speed υ recorded a series of photographs, and the point in time associated with the ith photo could be calculated as $\sim d_i/\upsilon$, where d_i was the distance from the starting gate to the ith camera. The separation in time between frames was $\tau = \Delta d/\upsilon$, where $\Delta d = d_{i+1} - d_i$, so the number of frames per second was $\upsilon/\Delta d$. Although the absolute timing of the frames of the series was imperfect, tied as it was to the velocity of the horse from camera to camera, the images nevertheless permitted detailed analysis of the motion. The imprecision of the chronology of images obtained in this manner was subjected to some criticism, and in his later studies, Muybridge used cameras with shutters triggered sequentially by a clockwork mechanism (*2*) to obtain photographs regularly spaced in time, such as those shown in Figure 2.

Etienne-Jules Marey, professor at the Collège de France and a contemporary of Muybridge, invented "chronophotography", a reference to the regular timing of a sequence of images (*2, 3*) recorded by a *single* camera using a rotating slotted-disk shutter (the analogue of shutter-stroboscopy, the concept of which was developed as early as 1832; the related flash-stroboscopy is discussed in what follows). The recording was made on either a single photographic plate or a film strip, the precursor to modern cinematography. Marey, like Muybridge, focused on investigations of humans and animals in motion, such as the motion in righting of cats.

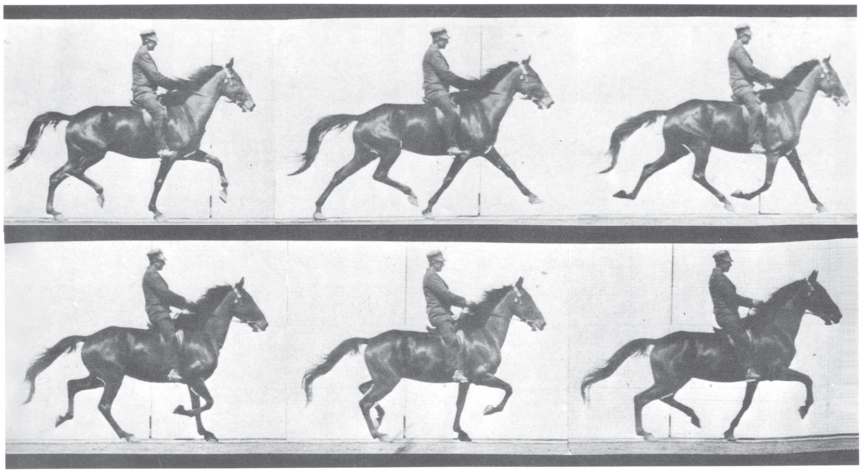

Figure 2. A series of photographs by Eadweard Muybridge of a trotting horse, taken during studies at the University of Pennsylvania (1884–1885). The time interval between photos is regular, 0.052 s. Note that in the third photograph (top right), all four hooves are simultaneously off the ground in the trot motion.

Muybridge also developed an apparatus to project sequences of images obtained in his experiments to give "the appearance of motion" in demonstrations representing an early stage in the development of motion picture technology. His device, which he called a zoöpraxiscope, made use of a projecting lamp and counter-rotating image and shutter disks to produce a rapid succession of apparently stationary bright images and periods of intervening darkness. With image frames appearing at a rate greater than about 20 per second, the viewer's perception of each bright image persisted across the dark intervals, merging with its successor to form the desired continuous, but moving, picture. A simpler device for viewing the sequences, which was well known in Muybridge's time, is the zoetrope (from the Greek *zoe* 'life' and *tropos* 'turning'). It consists of a cylinder spinning on its axis with a series of slits equally spaced around its circumference. Through the slits, photos on the opposite inner surface are briefly glimpsed in rapid sequence, giving an impression of continuous motion.

B. Stroboscopy

An alternative approach to the study of rapid motions, which has also proved capable of reaching much shorter time scales than possible with fast shutters, is the use of short light flashes, which make an object moving in the dark visible to a detector (observer's eye or photographic plate, for example) only during the light pulse. Thus the pulse duration Δt plays the same role as the opening of a camera shutter and can be thought of in just the same way. An instrument that provides a series of short light pulses is a stroboscope (*strobos* from the Greek word for "whirling" and *scope* from the Greek for "look at", for its original use in viewing rotating objects). Combined with a camera with an open shutter and with an appropriately chosen Δt for the light pulses, a stroboscope can produce a well-resolved image of an object as fast as a bullet.

In the mid-19th century, spark photography had been demonstrated for stopping rapid motions. The development of stroboscopic photography in the mid-20th century was greatly advanced by Harold Edgerton, professor at MIT and cofounder of EG&G electronics, through the development of electronic flash equipment capable of producing reliable, repetitive, and microsecond-short flashes of light. (Edgerton and EG&G also developed camera shutters based on optical principles with no moving parts that are far faster than any conventional mechanical shutter [*3*].)

An example of the use of a stroboscope is shown in Figure 3, a precisely timed sequence of images of a falling apple. With the apple's velocity limited to $v \leq 5$ m/s and a value of Δx of ~1 mm for a sharp image, Δt of the flash must be ~(1 mm)/(5 m/s) = 2×10^{-4} s or less, well within the stroboscope's range. An absolute time axis is established here by electronic timing of the flashes. The picture shows the effect of gravity, which can be quantified by analyzing the successive positions in which the light illuminates the apple. According to the law of uniformly accelerated motion

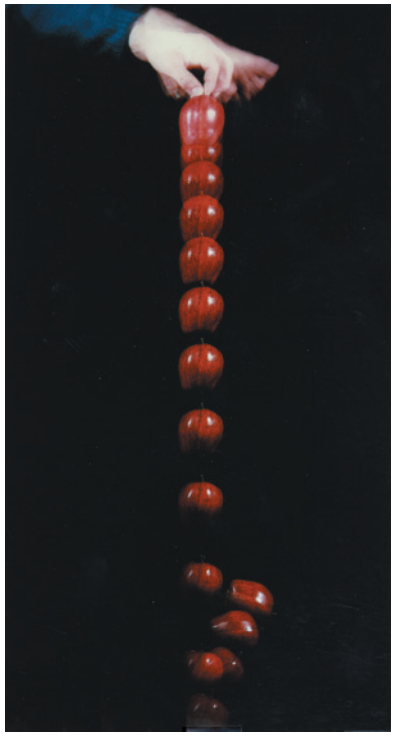

Figure 3. A falling apple photographed by stroboscopic illumination at intervals of ~1/25 s (*3*). The effect of gravity is clear.

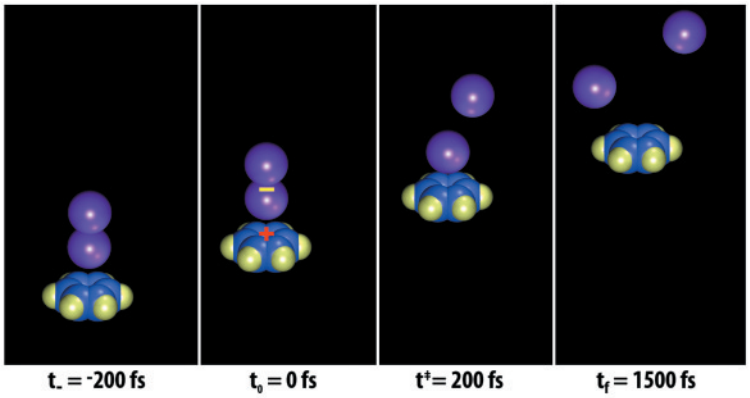

Figure 4. Molecular structures for a reaction in progress involving two molecules (bimolecular). The diatomic iodine molecule (I_2, top) is split by exchange of an electron with the ring molecule benzene (C_6H_6).

$x = \frac{1}{2} a t^2$, for the position x of an object at rest at $t = 0$ and subjected to acceleration a. Therefore, flashes equally spaced in time record images of uniformly increasing separation (up until impact and rebound from the table); the slope of the plot of image separation versus time is equal to $g\tau$, where g is the acceleration of gravity (~9.8 m/s^2) and τ is the spacing of the flashes. When an apple height of 10 cm is assumed in Figure 3, one finds that τ is ~0.04 s; that is, the strobe flash rate was ~25 per second.

C. Femtoscopy

If the above ideas can be carried over in a straightforward manner to the study of atoms in motion, then the requirements for a femtochemistry experiment are easily determined. For a molecular structure in which atomic motions of a few angstroms typically characterize chemical reactions, a detailed mapping of the reaction process will require a spatial resolution Δx of less than 1 Å, more than 8 orders of magnitude smaller than needed by Muybridge. Therefore, the Δt required to observe with high definition molecular transformations in which atoms move at speeds of the order of 1000 m/s is (0.1 Å)/(1000 m/s) = 10^{-14} s = 10 fs. While this time scale has been recognized theoretically as the time scale for chemical reactions since the 1930s, it became possible to directly see the detailed steps in molecular transformations for the first time in the 1980s (*4*) with the development of femtosecond lasers (see Appendix). Such minute times and distances mean that molecular-scale phenomena are governed by quantum mechanical principles. Quantum theoretical considerations that are fundamental to the observation of atoms in motion are discussed in Section IV.

Flashing a molecule with a femtosecond laser pulse can be compared to the effect of a stroboscope flash or the opening of a camera shutter. Thus a pulse from a femtosecond laser, combined with an appropriate detector, can produce a well-resolved "image" of a molecule as it passes through a specific configuration in a process of nuclear rearrangement, as Muybridge caught the horse with all four feet in the air. (The detection step is based on spectroscopic or diffraction techniques, and the measured signal can be analyzed to give information about the positions of the molecule's atoms; see Appendix.) The pulse that produces such an image is called a *probe* pulse, because it is used to probe the molecule's structure just as a shutter opening and a stroboscope flash probed the positions of the horse and apple in Figures 2 and 3, respectively. The use of laser pulses to "stop the motion" of atoms and obtain instantaneous molecular structures may be called femtoscopy; femto, the prefix meaning 10^{-15}, is from *femton*, the Scandinavian word for "fifteen". Molecular structures determined at different stages of a reaction process can be treated as the frames of a motion picture, allowing the motion of the atoms to be clearly visualized, as illustrated in Figure 4; the number of frames in a molecular movie could then be as high as 10^{14} per second.

Probing is not the whole story. For the entire course of any motion to be recorded, that motion must be initiated so that it takes place in the time span accessible to a sequence of probe snapshots. In photographing the horse and apple, the processes are initiated by opening a starting gate for the horse and by releasing the apple, and the respective probing sequences are arranged to coincide closely in time to those actions. For femtochemistry, the analogous operation is realized by launching the molecule on its path using a femtosecond initiation pulse (the *pump* pulse) passing through the sample. This establishes a temporal reference point (time zero) for the changes that occur in the molecular motion or reaction. The timing relative to the probe pulses is accomplished by generating the pump and probe pulses from a common source and sending either the pump or the probe along an adjustable optical path to the sample (Fig. 5A). The difference between pump and probe path lengths divided by the constant speed of light of about 300,000 km/s (actually 299,792 km/s) precisely fixes each probe image on the time axis established by the pump.

Such use of optical path differences to measure transient phenomena dates back at least to 1899, when Abraham and Lemoine reported their measurement in France of the Kerr response of carbon disulfide (Fig. 5B) (*5*). They used the breakdown of air at a spark gap to *simultaneously* ($t = 0$) create a probe light pulse (spark) and discharge a parallel plate capacitor immersed in carbon disulfide. Before the discharge of the capacitor, the carbon disulfide molecules between the plates retained a net alignment with the applied electric field, resulting in optical birefringence, a difference in refractive index for light polarized parallel or perpendicular to the plates (Kerr effect). Upon discharge, the spark-produced probe light monitored the Kerr effect as a function of time by traversing a variable-length optical delay before passing between the plates of the capacitor. Polarization analysis showed that the substantial Kerr effect to which the probe light was subject at the shortest measurable delays was progressively reduced and

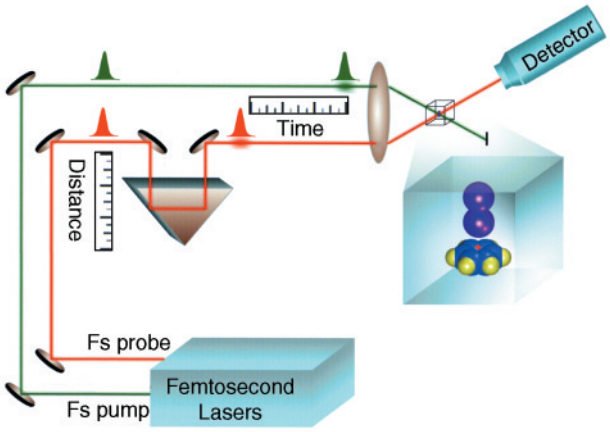

(A) The concept of femtosecond (pump-probe) experiments. After the probe pulse has been delayed by diversion through a variable-length optical path, femtosecond pump and probe pulses are focused into a volume containing the molecules to be studied. The detector responds to the probe pulse by any of a variety of schemes (see Appendix).

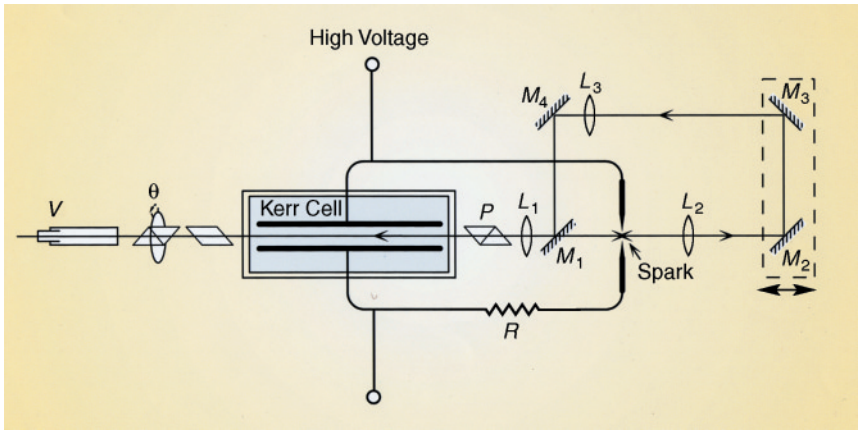

(B) Kerr-cell response measurement of Abraham and Lemoine (1899). The high voltage applied across the plates of the capacitor induce a Kerr effect in the carbon disulfide. The breakdown of air at the spark gap discharges the capacitor and creates a pulse of light, which follows the path indicated (reflecting from mirrors M_2, M_3, M_4, and M_1; L_2, L_3, and L_1 are collimating lenses) to probe the Kerr effect. The time dependence of the effect is determined by moving mirrors M_2 and M_3 as indicated, to vary the time delay for passage of the probe pulse through the Kerr cell. The light is polarized before the cell by the polarizer P, and the Kerr effect is quantified by adjusting the rotation angle θ of an analyzing polarizer to measure the polarization properties of the light after passage through the Kerr cell, as observed at the viewing telescope V.

Figure 5. Experimental layouts using changes in optical path length to establish timing.

ultimately disappeared as the delay path length was increased. From this observation, a half-life of 2.5 nanoseconds, corresponding to a path length of 75 cm, was determined for the combined electrical and Kerr (alignment) response time of the system. We now know that the Kerr response due to reorientation of the molecules occurs in ~2 ps (1 ps = 10^{-12} s), with a femtosecond component associated with electronic polarization effects.

A fundamental difference between femtoscopy and the horse and apple analogies is that, in femtochemistry experiments, one probes typically millions to trillions of molecules for each initiation pulse, or repeats an experiment many times, to provide a signal strong enough for adequate analysis. A comparable situation would arise in stroboscopy of the apple if capture of a distinct photographic image could only be accomplished by using many different apples or repeated exposures. It is clear that success in such a case would require (i) precise *synchronization* of the strobe (probe) pulse sequence with the release of the apple, to less than or about the strobe pulse duration, for optimum resolution; and (ii) a precisely defined launching configuration of each apple, to a fraction of an apple diameter.

By the same reasoning, to synchronize the motion of many independent *molecules* so that all have reached a similar point in the course of their structural evolution when the probe pulse arrives to capture the desired impression, the relative timing of pump and probe pulses must be of femtosecond precision, and the launch configuration must be defined to subangstrom resolution. It is only by means of such synchronization that the signals from many molecules may be added together without hopelessly blurring the molecular structure derived from the measurement. The use of pulses generated from the same source and an optical path delay as described above provides the required high degree of timing precision. A typical optical path accuracy of 1 μm corresponds to absolute timing of the molecular snapshots of 3.3 fs (see Fig. 5A).

Of equal importance is the required definition of the launch configuration. This definition is naturally realized because the femtosecond pump pulse snaps all members of the molecular ensemble from their ground states, which have a single well-defined structure. Moreover, on the femtosecond time scale, moving atoms are coherent or particle-like in their trajectories. The quantum description of how the localiza-

tion of nuclei in motion is achieved in the molecule and the ensemble is discussed in Section IV.

III. Demonstration

Because the scales of distance and time of the motions that are the subject of femtochemistry research are almost unimaginably small and the measured signals require a sophisticated apparatus and analysis of data, we have, for educational purposes, designed a simple exhibit capable of highlighting the basic concepts of femtochemistry and stop-motion stroboscopy. The exhibit gives a student or visitor a concrete and visually interesting illustration of the use of short light pulses in the study of a rapidly moving object, in this case a molecular model.

The exhibit occupies a 3 × 5-ft table (Fig. 6, top). The output of a continuous-wave, diode-pumped solid-state laser (532 nm, 15 mW; appropriate safety precautions should be observed in handling such laser powers) is chopped by a rotating opaque disk 6 cm in radius provided with two openings (4.8 cm and 5.1 cm from the rotation axis), of tangential lengths 2 mm and 8 mm, respectively. The chopper is rotated by a dc motor (driving voltage 0–12 V, 2600 rpm at 4.5 V) and is mounted on a translation stage allowing either of the two openings to be positioned in the optical path.

The chopped laser beam passes through three lenses at ~3-inch spacing: two strongly diverging lenses (ca. −25 mm focal length each) and a 2-inch diameter 300-mm focal length converging lens. These lenses expand the 1-mm diameter beam into a gently diverging light cone (~6° divergence) of 7-cm diameter at a distance of 40 cm from the last lens. At that point the light illuminates a molecular model (here, methane, 5-cm diameter) mounted on the axle of a second dc motor. After an additional 40-cm path length the light is reflected by a plane mirror toward a screen at a distance of 60 cm from the mirror. The shadow of the model cast on the screen by the laser light is about 3 times the size of the model. The camera in the exhibit is representative of the detection step in a real experiment.

When the molecular model (Fig. 6, bottom, far left) is set in rapid rotation (frequency $\nu > 10$ Hz), it appears only as a blur to the eye if viewed under continuous illumination (Fig. 6, bottom, second from left), and a blurred shadow is cast on the screen if the laser is not chopped. With pulsed laser illumination, we can freeze the motion for study in the manner discussed in the previous section, if the spatial resolution and timing requirements can be satisfied. First, the model atoms are about 1 cm in dimension, so the spatial resolution needed to produce a sharply defined image is $\Delta x \approx 1$ mm. The linear speed υ of an atom moving across the laser beam

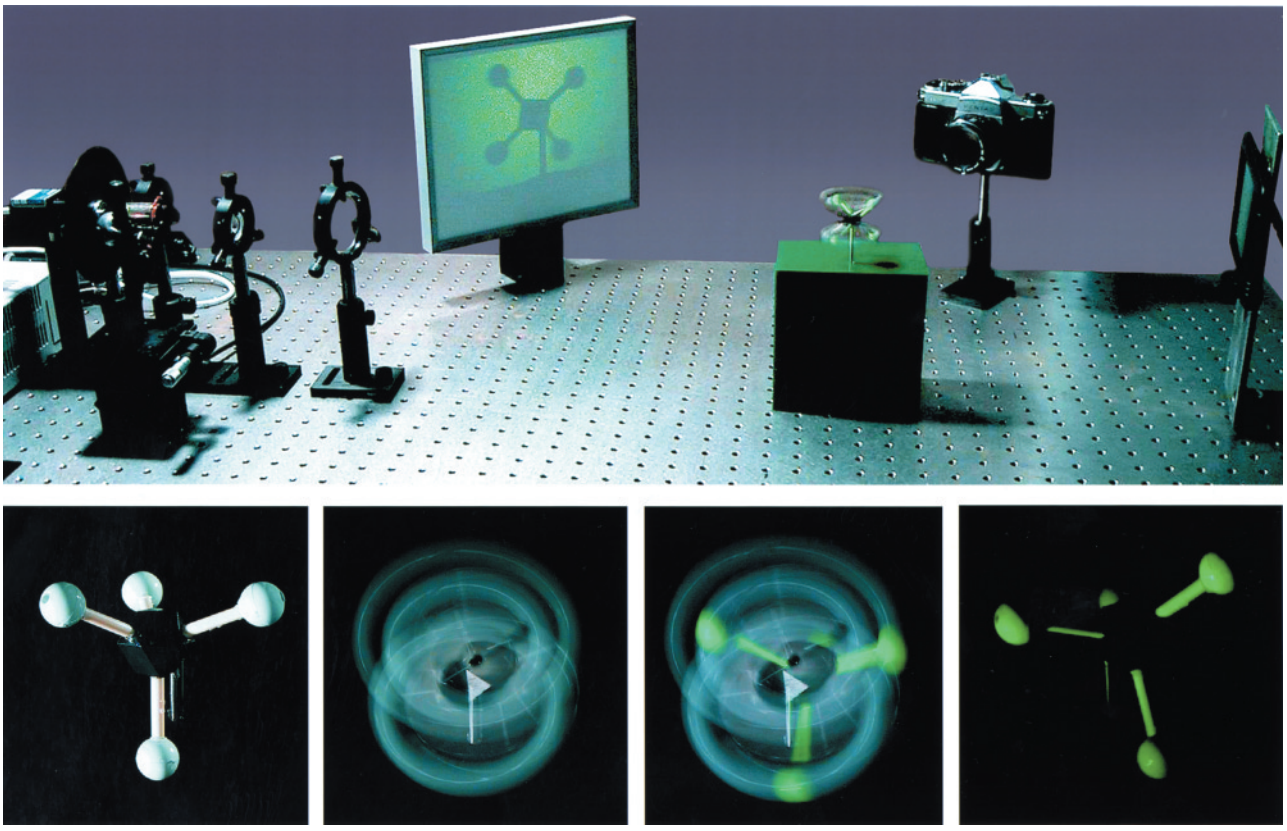

Figure 6. The laser demonstration. Top: Exhibit overview. A continuous green laser at far left is chopped by a chopper wheel, passes through three lenses, illuminates a spinning molecular model, and is reflected by the mirror at far right to the screen at center left. Bottom: Four views of the molecular model are. From left to right, the model is (1) stationary under room light only; (2) spinning under room light only; (3) spinning under room light and pulsed laser illumination; and (4) spinning under pulsed laser illumination only.

may be calculated from the relation $\upsilon = \omega r$ for a point at distance r from the rotation axis of a body rotating at angular velocity ω. For r_{max} = 2.5 cm and ν = 43 Hz (~2600 rpm), $\omega = 2\pi\nu$ = 270 rad/s and υ_{max} = 675 cm/s. Therefore, the first requirement of the exhibit laser pulses is that their duration Δt be $\leq$ (0.1 cm)/(675 cm/s) = 1.5×10^{-4} s = 150 μs to produce a sharp image or cast a distinct shadow.

The synchronization by the pump pulse in femtochemistry is necessary to allow a well-defined image constituted from many independent molecules, as discussed above. Similarly, in the exhibit, the observer can study a persistent image or shadow of the object only when the model is rapidly and repetitively exposed to the laser flashes in precisely the same spatial configuration. Otherwise, even when each pulse is short enough to produce an isolated sharp image, the rapid sequence of different and fleeting images will leave a blurred or chaotic impression on the eye. Since the rotating model undergoes a periodic motion, it will always be at the same point in its trajectory as the probe pulse arrives when the frequency (repetition rate) of the probe pulses created by the chopper wheel is adjusted to match the frequency of rotation of the model. The resulting sequence of synchronized, identical images can then be viewed *as though the molecule were stationary*.

The two right-hand photos of the spinning model at the bottom of Figure 6 show this effect with and without room lights. The enlarged shadow cast on the screen appears likewise as the shadow of a stationary object (Fig. 6, top). Note that stationary *multiple* images of the model can also be produced by many other chopper frequencies not equal to the model rotation frequency. For example, when the chopper frequency is 3/4 of the rotation frequency, the model is illuminated every 4/3 rotation, giving three stationary overlapping images separated from each other by 120° rotations.

By tuning the voltage driving the motor of the chopper and observing the model or its shadow, the synchronization condition to observe a single stationary image can be found. The pulse duration Δt is then fixed by the length of the aperture. To illustrate the role of pulse duration in determining image definition, there are apertures of different lengths in the wheel. With the chopper wheel rotating at 2600 rpm, $\Delta t \approx$ 150 μs is obtained when the laser passes through the 2-mm aperture. As determined in the calculation above, these 150-μs pulses give a sharp image of the molecule. Translation of the chopper to let the laser pass the 8-mm opening at slightly larger radius on the chopper disk results in a train of 580-μs pulses. With these pulses, the structure of the molecule is still easily distinguishable, but it is somewhat blurred rather than sharply defined.

We note that with the setup as described, only ~0.38 mW (2.5% of the laser light) and ~0.1 mW pass the 8-mm and the 2-mm aperture, respectively. These power levels of 532 nm light allow the stroboscopic effect to be visible in ambient illumination. For comparable visibility, a 60-mW red helium–neon laser would be required, since the relative visibility of light is ~3.8 times higher at 532 nm than at 633 nm. If desired, a laser of lower visibility can be used for the exhibit in an appropriately darkened environment. Indeed, the use of a laser is not critical, and any sufficiently bright light source, either a conventional continuous-wave light with chopper or a pulsed light (strobe) with adjustable pulse lengths, may be substituted.

IV. Femtochemistry—Principles and Applications

Up to this point, in applying the principles of stroboscopy to the molecular realm, we have treated the motion of atoms no differently from those of macroscopic objects like horses or apples. These latter objects of everyday experience are governed by what are known as the classical mechanical laws of motion, due to Newton, in which each body has a well-defined position and velocity at any time. However, when dealing with the actual molecular scale of motions in a femtochemistry experiment, quantum mechanical concepts become of paramount importance. Specifically, at the scale of atomic masses and energies, the quantum mechanical particle–wave duality of matter comes into play, and the notions of positions and velocities common to everyday life must be applied cautiously. In this section, we will first examine how the principles of quantum mechanics and uncertainty apply in the world of molecules, then show how on the femtosecond time scale it is nevertheless appropriate to describe atomic motion classically—the atoms move like localized particles with well-defined velocities. Examples of the behavior of real molecular systems are given.

A. Matter Particle–Wave Duality and Concept of Coherence

One of the profound findings of quantum mechanics is the particle–wave duality of matter expressed by the remarkable relationship of de Broglie in 1924: $\lambda = h/p$, where λ is the de Broglie matter wavelength, h is the Planck constant, and p is the momentum of the particle/wave, $p = m\upsilon$. In wave mechanics, the state of any material system is totally defined by a spatially varying wave function from which it is possible to determine only *probabilities* of the system's having a certain spatial configuration or having a certain momentum, rather than specific values for those quantities. For example, the probability that a particle whose wave function is $\Psi(r,t)$ will be found at position r is $|\Psi(r,t)|^2$, the square modulus of the wave function.

The form of wave functions representing atomic motion is determined by the energy landscape of the system, called the potential energy surface, which in a molecule depends on the specific arrangement of electrons around the nuclei. The total energy of an isolated system is constant, and the difference between the total energy and the potential energy is energy of motion, or kinetic energy (E_{kin}), of the constituent particles. The classically allowed region of the potential energy landscape of a system consists of all regions in which the total energy is greater than the potential energy; that is, where E_{kin} is nonnegative. According to classical mechanics, motion of the system is only possible in this region. If the classically allowed region is limited in extent (i.e., the system is confined or bound), only certain specific values of the energy are possible.

When the energy of a system is exactly defined (energy uncertainty $\Delta E = 0$), its wave function spreads over (and even somewhat beyond) the entire classically allowed region of space, and the position probability density (ppd) is independent of time. Mathematically, the spatial and temporal dependence of the wave function are separable, and $\Psi(r,t)$ may be written as $\Psi(r,t) = \psi(r) \exp(-iEt/\hbar)$, where the position-independent temporal phase factor, $\exp(-iEt/\hbar)$, is a complex number of

modulus 1. Thus

$$|\Psi(r,t)|^2 = \psi(r)\exp(-iEt/\hbar)\,\psi^*(r)\exp(iEt/\hbar) = |\psi(r)|^2$$

with no time dependence.

To illustrate these concepts, we present in Figure 7 the simple case of a diatomic molecule vibrating in a parabolic, or harmonic, potential energy well, which is an approximate representation of the vibrating iodine molecule. The horizontal axis represents the separation, r, of atomic nuclei. The possible energy values of the system are represented by the horizontal lines labeled by the quantum number n. Examples of wave functions $\psi_n(r)$ corresponding to n = 0 and 16–20 are plotted, with the zero of the wave function amplitude axis set equal in each case to the corresponding energy value. The sign of the wave function alternates from positive to negative with a spatial period determined by the kinetic energy, which is zero at the walls of the well and has its maximum value at the center.

When the physical state of a molecule is described by one of these wave functions of definite energy, a measurement of atomic position will reflect only the stationary probability distribution, with no nuclear motion. Taking n = 20 of Figure 7, for example, there are 21 peaks in the ppd (corresponding to both positive and negative peaks in the wave function), distributed from one wall of the potential to the other. As another example, the ppd and the momentum probability distribution for a stationary state of a more realistic potential, one modeled on the quasi-bound excited state of sodium iodide (NaI) (see below), are shown in Figure 8. The ppd fills the classically allowed region of the potential well, from 2.75 Å to 10.19 Å, and the momentum probability has peaks that correspond to the kinetic energy (~5300 cm^{-1}; 1 cm^{-1} = 1.98648×10^{-16} ergs) near the center of the well.

Motion is observed in ultrafast laser experiments when the system is prepared in a *coherent* (*superposition*) *state*, making the state function a coherent sum of stationary wave functions for different energies E_i:

$$\Psi(r,t) = \sum_i c_i\,\psi_i(r)\exp(-iE_it/\hbar) \qquad (1)$$

The coefficients c_i determine the relative contributions of the wave functions to the superposition. The sum is said to be coherent when well-defined phase relations exist between the constituent wave functions (see below). The ppd in this case is simply

$$\Psi(r,t)\,\Psi^*(r,t) = \left[\sum_i c_i\,\psi_i(r)\exp(-iE_it/\hbar)\right]\left[\sum_j c_j^*\,\psi_j^*(r)\exp(+iE_jt/\hbar)\right] \qquad (2)$$

One can see that cross-terms ($i \neq j$) in this product are *not* time independent (the phase factors do not cancel), but oscillate at the frequencies determined by the energy differences ($E_i - E_j$), so the expected outcome of a position measurement changes with time—*the system is in motion*!

B. Analogy with Light

The above is an example of wave superposition and *interference*, a more familiar example of which is the Young double-slit light interference experiment, illustrated at the bottom of Figure 7. As the wave function is a probability wave, so light is a wave of electric and magnetic fields whose amplitudes change at a regular interval, the wavelength, from positive to negative to positive along the direction of propa-

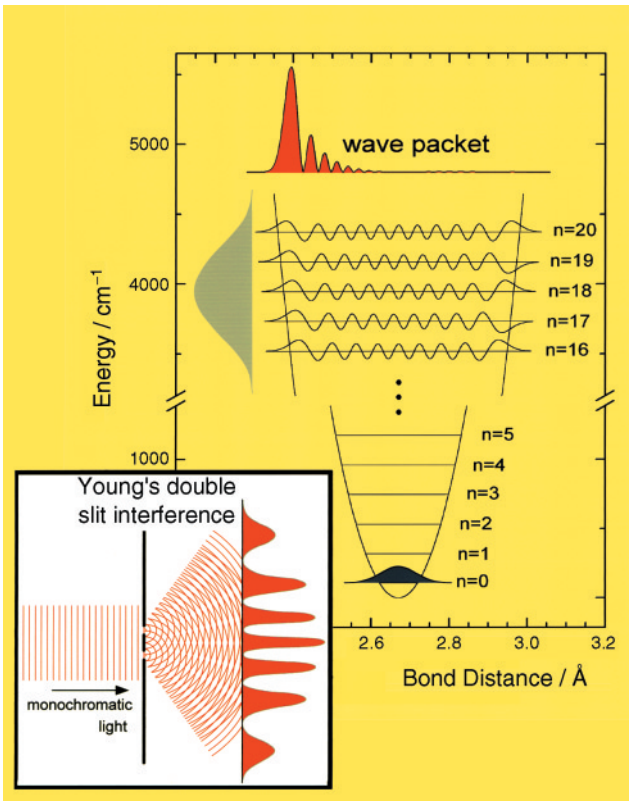

Figure 7. Diatomic molecule in a harmonic oscillator potential: stationary wave functions and formation of a localized wave packet. Inset: Thomas Young's experiment (1801) on the interference of light.

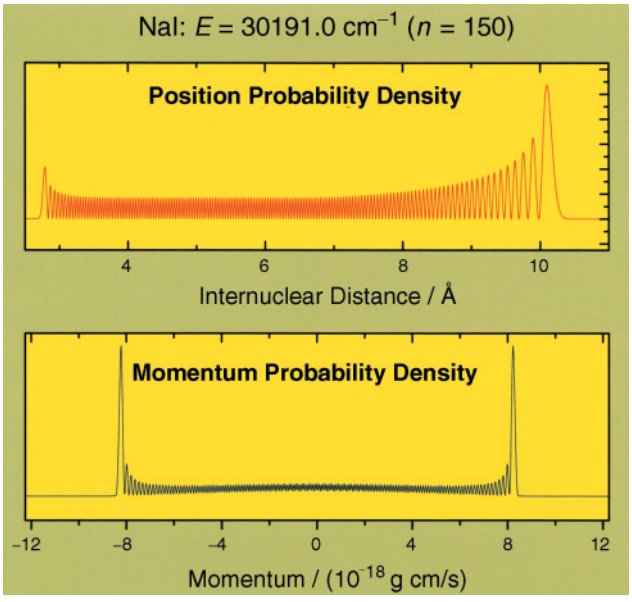

Figure 8. Stationary state of the theoretical bound potential of NaI (modeled on the real quasi-bound potential that is covalent in nature at short distances and ionic at long distance)—position and momentum probability distributions.

gation. Like the ppd, the intensity of light at a point in space is given by the square of the field amplitude. When light from two or more sources overlaps in space, the instantaneous field amplitudes (not intensities) from each source must be added together to produce the resultant light field.

In Thomas Young's two-slit experiment, reported in 1801, light from a single source passes through two parallel slits cut in an opaque screen to produce, in the space beyond, two *phase-coherent* fields of equal wavelength and amplitude. At points for which the distances to the two slits differ by $n + \frac{1}{2}$ wavelengths (for integer n) the amplitudes of the two superposed fields are opposite in sign and add to zero at all times; no light is detected. Elsewhere, the amplitudes do not cancel. Thus, a stationary pattern of light and dark interference fringes is produced. If, instead, *incoherent* (without a well-defined phase relation) fields of the same amplitudes were superposed, the intensities observed from each slit individually would simply add together and no interference fringes would be seen.

C. Wave Packets and Uncertainty—the Classical Limit

In a manner analogous to the interference of light waves in the Young experiment, the constituent matter wave functions of a coherent superposition state interfere constructively and destructively, and the resultant total wave function may have a large amplitude in only a limited area of the classical region at any given time. This constitutes a *wave packet*. At the top of Figure 7 is shown a specific example of the ppd of a wave packet formed from a superposition of the plotted wave functions n = 16 to 20 with weighting according to the distribution curve at the left of the figure. As time advances ($t > 0$ in $\exp(-iE_it/\hbar)$), the phase relationships between wave functions change, causing the wave packet to move. As long as the ppd remains sufficiently localized on the scale of the total classical region, as it is in the figure, a discussion in terms of the classical concepts of particle position and momentum is entirely appropriate. Such is the case for the wave packet of Figure 7, which will oscillate back and forth across the potential well indefinitely as would a classical particle at the same energy in that potential.

For a laser pulse to prepare a system in a localized wave packet, the deposited energy cannot be precisely defined, as wave functions at a broad range of energies E_i must be included in the superposition state. Given that the sizes of the energy quanta of a radiation field are determined by the constituent wavelengths, this translates into a requirement for a broad range of wavelengths in the field, which is also consistent with the nature of ultrafast pulsed laser sources. (Ultrashort light pulses are produced much as wave packets are formed, by coherently combining a large number of different wavelengths of light, each corresponding to a characteristic mode of the laser cavity; see Appendix.) Thus localization in time and in space are simultaneously achievable by virtue of the energy uncertainty!

When the extent of the classically allowed region is unbounded, the energy may take on all values rather than being restricted to quantized levels, but the same principle of superposition of wave functions applies to building wave packets; the sum in eq 1 becomes an integral. One example of unbound motion is motion at constant potential energy—that is, for a *free particle*. It is possible in this case to create a wave packet in one dimension with a very simple bell-shaped spatial profile defined by the Gaussian equation

$$\Psi(x,t) = N(t)\exp\left(-\frac{(x - x_0 - \langle\upsilon\rangle t)^2}{4[\Delta x(t)]^2}\right) \qquad (3)$$

where $\Delta x(t)$ can be shown to be the root mean square (rms) deviation in the ppd, $|\Psi(x,t)|^2$, and $N(t)$ is a normalization constant. (The rms deviation of a probability distribution $P(x)$ is given by

$$\left[\int_{-\infty}^{+\infty}(x-\bar{x})^2P(x)\mathrm{d}x\right]^{1/2}$$

where $\bar{x}$ is the mean value $\int_{-\infty}^{+\infty} xP(x)\mathrm{d}x$.) The time dependence of Δx is considered below. The maximum of the wave function or ppd is at $x_0 + \langle\upsilon\rangle t$ and thus moves at velocity $\langle\upsilon\rangle$. Note that the full width at half maximum (FWHM) of a Gaussian function is $2(2\ln 2)^{1/2} = 2.3548$ times its rms deviation, so the full width, $\Delta x^{\mathrm{FW}}(t)$, of the ppd is equal to $2.3548 \times \Delta x(t)$.

The well-known Heisenberg uncertainty relation states that the degree of localization in space of a quantum system is inversely related to the minimum uncertainty in the system's momentum. That is, the more limited the extent of the ppd $|\Psi(x,t)|^2$, the larger the uncertainty in the momentum, and thus the less well defined the future trajectory can be. When the uncertainties Δx and Δp are defined as rms deviations of the probability distributions, then the uncertainty relation is $\Delta x\,\Delta p \geq \hbar/2$, where $\hbar = h/2\pi$.

For a Gaussian free particle wave packet having the minimum value of the uncertainty product, $\Delta x\,\Delta p = \hbar/2$, the momentum distribution is also Gaussian, and the contribution of the momentum uncertainty to the widening of the packet as it moves is expressed in the relationship

$$\Delta x(t) = [\Delta x^2(t=0) + (\Delta\upsilon \times t)^2]^{1/2} \qquad (4)$$

where $t = 0$ is the time of minimum uncertainty and $\Delta\upsilon = \Delta p/m$. Because Δp is inversely related to $\Delta x(0)$, it is only possible to slow the spreading by an increase in the initial Δx, thereby allowing a smaller $\Delta\upsilon$. Note that spreading is inevitable for the minimum-uncertainty, free-particle wave packet, but not for wave packets in general, which can be shaped by their potentials. Equation 4 can be used to give a feeling of the time needed for an appreciable spreading to take place—for $\Delta x(t)$ to increase by a factor of $\sqrt{2}$, the product $\Delta\upsilon \times t$ must be equal to $\Delta x(t = 0)$. From this equality and the uncertainty relation for rms deviations, we can express t_s, the time for spreading by ~40%, as

$$t_s = \Delta x(0)/\Delta\upsilon = m\Delta x(0)/\Delta p = 2m\Delta x^2(0)/\hbar \qquad (5)$$

When a free particle wave packet is initiated by an ultrashort light pulse so that it has the minimum value of the $\Delta x\,\Delta p$ uncertainty product, one can calculate the relation between the pulse duration and the wave-packet spatial width. It turns out to be quite simple: $\Delta x = \langle\upsilon\rangle\Delta t$.

The size of $\hbar$, 1.05457×10^{-27} erg-second, means that the fuzziness required by the uncertainty principle is imperceptible on the normal scales of size and momentum, but becomes important at atomic scales. For example, if the position of a stationary 100-g apple is initially determined

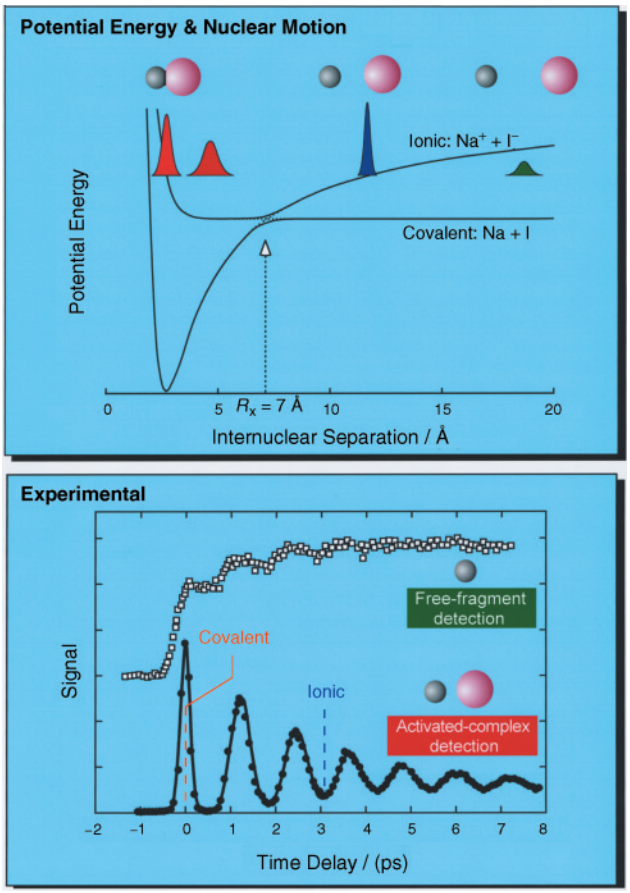

Figure 9. Femtoscopy of the bond breakage and bond reformation of sodium iodide. Top: The two potential energy functions, the two channels of wave packet evolution (bound and free), and schematic of wave packet motion. Bottom: Time sequence of measured populations of free fragments (open squares) and of quasi-bound complex transition-state configurations (see Appendix).

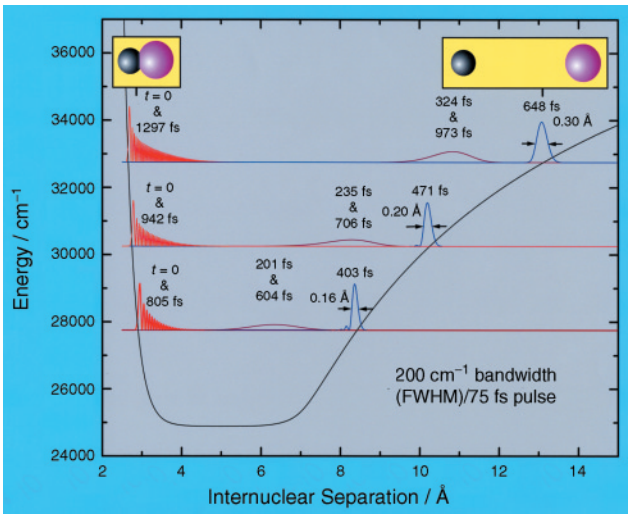

Figure 10. Evolution of a 200-cm^{-1} FWHM bandwidth wave packet, corresponding to pulses of 73.6-fs (~75-fs) FWHM, on the theoretical bound potential of NaI (see legend to Figure 8) at three excess energies: 2862, 5362, and 7862 cm^{-1}.

to a small fraction of a wavelength of light, say Δx = 10 nm, a momentum uncertainty greater than

$$\frac{\hbar/2}{\Delta x} = \frac{0.5 \times 10^{-27}\ \text{erg-s}}{1 \times 10^{-6}\ \text{cm}} = 5 \times 10^{-22}\ \text{g cm/s}$$

will be imposed, or $\Delta\upsilon \geq 5 \times 10^{-24}$ cm/s. Under the minimum uncertainty assumption, eq 5 can be used to calculate that the apple's position uncertainty will spread by ~40% only after 2×10^{17} s, or 6 billion years! On the other hand, an electron with a mass 29 orders of magnitude smaller would spread by 40% from an initial 1 Å localization after only 0.2 fs. Clearly, the much greater masses of atomic nuclei make their wave packets spread orders of magnitude slower than the wave packet of the electron (see below).

As mentioned in Section II C, atomic-scale localization is critical for femtoscopy: not only localization of the wave packets formed in each molecule, but of the total spread in position among wave packets formed in the large number of molecules on which the measurement is performed. When both types of spread are small with respect to the relevant extent of the classical region, the conditions for observation of a classical *single-molecule trajectory* have been met. The key to achieving localization of the molecular ensemble is generally provided by the naturally well-defined initial equilibrium configuration of the studied molecules before excitation by the pump pulse. For example, most iodine molecules at room temperature or below are in their n = 0 vibrational state, the wave function of which, shown in Figure 7, yields a width of the ppd of only 0.08 Å FWHM. This spatial confinement establishes the phase relations between the excited wave functions that produce and define the localized wave packets, so the entire sample of molecules are launched from essentially the same starting point—a single-molecule trajectory is observed. The femtosecond time resolution is critical to exploit this localized launch configuration before the dispersion or propagation of the wave packet.

D. A Paradigm Case Study—Sodium Iodide

Observation of the motion of nuclei as wave packets was realized in experiments conducted at Caltech in the 1980s. A prime example is represented by experiments on the wave packet motion of sodium iodide, and Figure 9 depicts the potential energy for the motion and the experimental observations. The quasi-bound upper potential curve is composed of a covalent inner part and an ionic long-range part created by the crossing of the covalent and ionic curves, as shown. As discussed below (see Appendix), the measurements show a large fraction of the excited wave packet oscillating in this well, between covalent and ionic bonding, while with each stretch a smaller fraction remains on the covalent surface and separates as free atoms. The role of coherence is critical in preparing the wave packet, and a single-molecule trajectory of the ensemble is assured when the pump pulse synchronizes all molecules near the 2.67-Å bond length of the ground state minimum at time zero. This system has been studied in great detail, highlighting these and other concepts, and it represents a paradigm case of molecular dynamics with atomic-scale

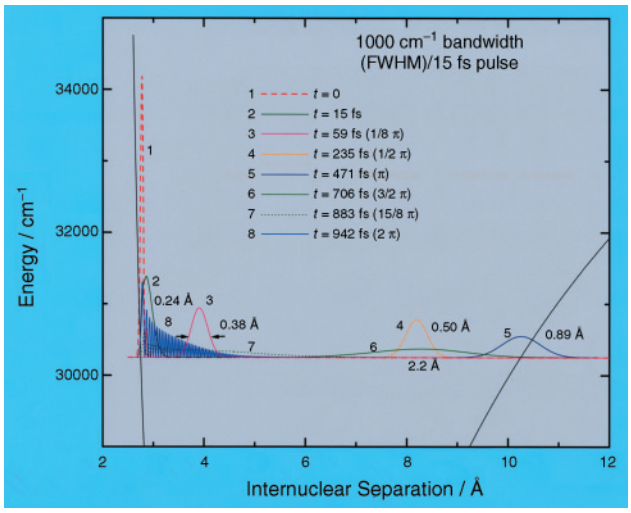

Figure 11. Evolution of a 1000-cm^{-1} FWHM bandwidth wave packet, corresponding to pulses of 14.7 fs (~15 fs) FWHM, on the theoretical bound potential of NaI (see legend to Figure 8) at 5362 cm^{-1} excess energy. Vibrational phase angles ($2\pi t/\tau_\upsilon$, where τ_υ is the vibrational period) are given in parentheses and the full widths at half-maximum for wave packets 2–6 are indicated.

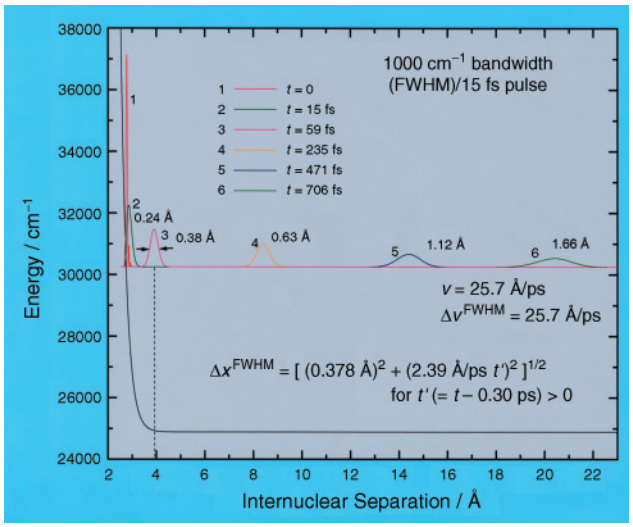

Figure 12. Evolution of a 1000-cm^{-1} FWHM bandwidth wave packet, corresponding to pulses of 14.7 fs (~15 fs) FWHM, for unbound NaI at 5362 cm^{-1} excess energy.

resolution (see ref *4* for more details). It is natural therefore to illustrate the properties and time evolution of wave packets as developed above with calculations based on the NaI system.

First, we give some examples of wave packet propagation on the theoretical bound state potential, which is modeled on the quasi-bound NaI state. This potential is shown in Figure 10, with an energy axis referenced to the NaI ground-state potential minimum. Five snapshots, representing one full vibrational cycle, of the ppd's of wave packets formed at three different center energies by coherent superpositions with 200-cm^{-1} FWHM Gaussian population bandwidths are also shown. (This bandwidth corresponds to ~75-fs FWHM laser pulses.) Note that the wave function whose ppd is shown in Figure 8 is one of the $\psi_i(r)$ contributing to the sum in eq 1 for the superposition at the middle energy, 30,250 cm^{-1} or 5362 cm^{-1} excess vibrational energy. At time zero, the constituent wave functions are all taken as real and positive at the inner turning point of the potential. As time advances, the phase factors, $\exp(-iE_it/\hbar)$, cause the wave packets to move, in each case broadening in the center of the well and sharpening at each turning point.

These wave packets are seen to remain well localized in comparison to the extent of the classically allowed region throughout their first vibrational periods. In fact, at this initial Δx, 10 or more vibrational cycles can be completed without the progressive spreading of the wave packet destroying the usefulness of a classical description of the motion. The femtochemistry experiments referred to above (Fig. 9), with pulses of similar duration, have shown this long-time particle-like behavior. In contrast, a calculation for a 1000-cm^{-1} FWHM bandwidth superposition, or ~15-fs pulse, at 5362 cm^{-1} excess energy, shown in Figure 11, is initially much more localized (smaller $\Delta x(0)$) but spreads much more quickly (larger Δp). Now the spreading of the wave packet in even one vibrational period is substantial.

As shown in Figure 9, the real NaI system involves two crossing potentials, one of which allows the Na and I to separate totally as free atoms. If we use the relative motion of Na and I at a constant potential as an example of free particle motion, for an average (kinetic) energy of 5362 cm^{-1}, the mean velocity of separation $\langle\upsilon\rangle$ is 25.7 Å/ps or 2.57 10^5 cm/s ($E_{kin} = \frac{1}{2}\mu\langle\upsilon\rangle^2$, where μ = 19.46 amu = 3.232 × 10^{-23} g, the reduced mass of Na and I). A 1000-cm^{-1} FWHM Gaussian energy bandwidth corresponds to a 14.72-fs FWHM Gaussian pulse. Such a pulse will create a minimum uncertainty wave packet of 0.378 Å FWHM. Restating the minimum uncertainty relation in terms of the full widths at half maximum as $\Delta x^{FW} \times \Delta p^{FW} \geq 8 \ln 2 \times \hbar/2 = 2.7726\hbar$, we can calculate a momentum spread Δp^{FW} of 7.73 × 10^{-19} g cm/s or $\Delta\upsilon^{FW} = \Delta p^{FW}/\mu$ = 2.39 Å/ps.

The growth with time of the wave packet spatial width can then be calculated from eq 4. Using FWHM values for the present case leads to

$$\Delta x^{FW}(t) = [(0.378\ \text{Å})^2 + (2.39\ \text{Å/ps} \times t)^2]^{1/2}$$

This gives a width of 2.4 Å after 1 ps. If the initial wave packet is twice as broad (0.756 Å), $\Delta\upsilon^{FW}$ will be half as large and the wave packet will spread more slowly, to only 1.4 Å after 1 ps. Twice the initial wave packet width will be produced for the same $\langle\upsilon\rangle$ by a pulse twice as long, or for the same pulse width by an average energy four times higher. Similarly, eq 5 can be used to calculate the time for the packet to spread by 40%: if $\Delta x^{FW}(0)$ = 1 Å, that is, $\Delta x(0)$ = (1/2.3548) Å , then t_s = 1.1 ps; the wave packet in that time travels over 28 Å. If $\Delta x(0)$ doubles, the wave packet takes 4.4 ps, four times as long, to spread by the same factor.

Figure 12 shows the evolution of an unbound NaI wave packet with energy spread corresponding to a 14.72-fs laser pulse. The wave packet is formed on the steep repulsive potential wall of the bound well, but evolves after the initial

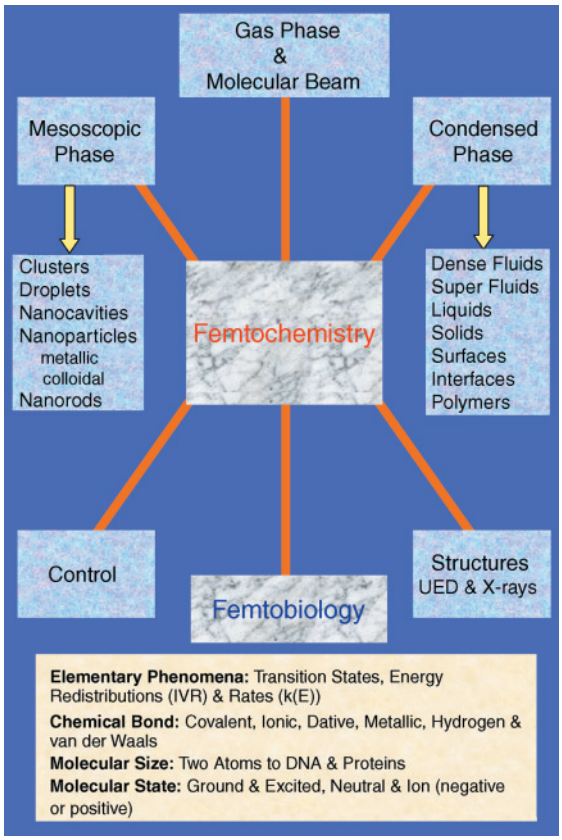

Figure 13. Scope of femtochemistry applications.

repulsion on the unbound, constant-energy surface. The initial packet is quite narrow and virtually identical to the bound packet of Figure 11; that is, its form depends only on the local potential surface. While the potential is changing sharply with distance ($t < 30$ fs) the above calculations concerning width and spreading of the wave packet for a constant potential energy are not applicable. However, after the packet enters the force-free region, it reproduces quite well the behavior predicted above for a free particle wave packet of minimum uncertainty at $t = 30$ fs.

These calculations for NaI show how, despite the important role of quantum uncertainty and wave mechanical behavior, it can be entirely appropriate to treat the nuclear motion of reacting molecular systems as particle-like, as we did in our presentation of the technique of femtoscopy.

E. World of Complexity

Femtochemistry is by no means limited to studies of small systems such as the two-atom system used as an example above. Femtochemistry has found applications in all phases of matter (Fig. 13) and in sibling fields including femtobiology of complex systems. For example, vision is the result of the conversion of light energy to an electrochemical impulse. The impulse is transmitted through neurons to the brain, where signals from all the visual receptors are interpreted. One of the initial receptors is a pigment called *rhodopsin*, which is located in the rods of the retina. The pigment consists of an organic molecule, retinal, in association with a protein named

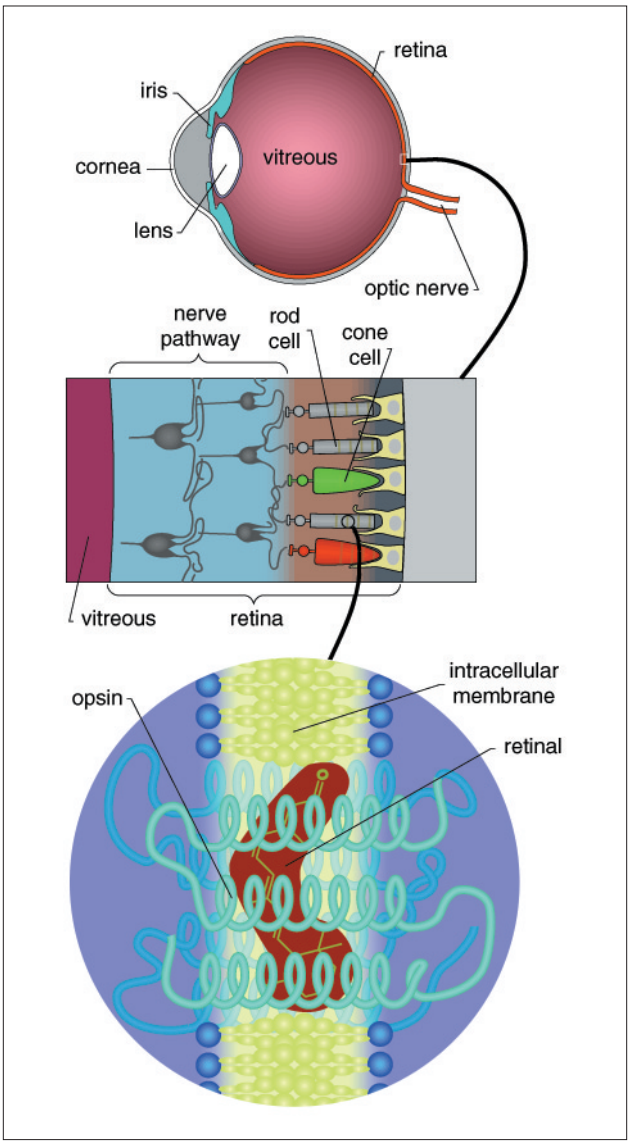

Figure 14. The molecular basis of vision. Within the light-sensitive rod and cone cells in the retina are membranes in which are embedded photoreceptive molecules such as rhodopsin, which comprises a light-absorbing part, retinal, and a protein, opsin. Top: simplified diagram of cross-section of the eye. Middle: enlargement of a portion of the retina, showing rod and cone cells. Bottom: schematic of part of a membrane within a rod cell. (Drawing by Randall J. Wildman.)

opsin (Fig. 14). A change in shape of retinal, which involves twisting of a double bond, apparently gives the signal to opsin to undergo a sequence of dark (thermal) reactions involved in triggering neural excitation.

The primary process of twisting takes 200 fs, similar to the time seen in prototypical chemical systems (stilbene); and coherent motion along the reaction coordinate continues after the reaction, in the photoproduct (*6*). The speed of the reaction and the product coherence indicate that the energy is not first absorbed, then redistributed to eventually find the reaction path; instead, the entire process proceeds in a coherent manner—that is, as a wave packet. This coherence is credited for making possible the high (70% or more) efficiency of the

initial step, despite the large size of the rhodopsin molecule and the many channels for dissipation of energy. These dynamics are similar to those of NaI, discussed above, even though the contrast in size is huge, from two atoms to a protein.

V. Conclusion

This paper presents an elementary description of the concepts basic to femtochemistry—the ability to freeze atoms in motion with femtosecond (10^{-15} s) time resolution. Unlike macroscopic motions, motion at the molecular scale requires new concepts to be addressed, and we elucidate the importance of coherence and the relationship to matter particle–wave duality and to the uncertainty principle. We provide a demonstration using a pulsed laser and molecular model to capture the fundamental idea behind the experimental technique. The exhibit is simple and can be made easily for educational and conceptual purposes. The analogy with stop-motion photography was highlighted over a century of development, from high-speed shutters to stroboscopes and on to femtoscopy; future directions include the use of ultrafast diffraction methods (*7*) to probe the totality of molecular structural changes in complex systems such as biological assemblies.

Acknowledgments

We thank the National Science Foundation for the support of this educational research. We wish also to thank the Nobel Museum Project (Stockholm) for triggering our interest in this effort, and Carsten Kötting and Dongping Zhong for help with three of the figures.

Literature Cited

1. von Baeyer, H. C. *Taming the Atom*; Random House: New York, 1992.
2. Muybridge, E. *Animals in Motion*; Dover: New York, 1957. See also Haas, R. B. *Muybridge*; University of California Press: Berkeley, 1976.
3. Jussim, E.; Kayafas, G. *Stopping Time*; H. N. Abrams: New York, 1987. See also Frizot, M. *La Chronophotographie*; Exposition á la Chapelle de l'Oratoire: Beaune, France, 1984.
4. Zewail, A. H. In *Les Prix Nobel (The Nobel Prizes 1999)*; Frängsmyr, T., Ed.; Almqvist and Wiksell: Stockholm, Sweden, 2000; pp 110–203 and references therein. A shorter version was published in *J. Phys. Chem., A* **2000,** *104*, 5660–5694.
5. Abraham, H.; Lemoine, J. *C. R. Hebd. Seances Acad. Sci.* **1899,** *129*, 206–208.
6. See: Wang, Q.; Schoenlein, R. W.; Peteanu, L. A.; Mathies, R. A.; Shank, C. V. *Science* **1994,** *266*, 422–424. For stilbene, see Pedersen, S.; Bañares, L.; Zewail, A. H. *J. Chem. Phys.* **1992,** *97*, 8801–8804.
7. Ihee, H.; Lobastov, V. A.; Gomez, U. M.; Goodson, B. M.; Srinivasan, R.; Ruan, C.-T.; Zewail, A. H. *Science* **2001,** *291*, 458–462.
8. Hopkins, J.-M.; Sibbett, W. *Sci. Am.* **2000,** *283* (3), 73–79, and references therein. References 18 and 19 in *Les Prix Nobel* (*4*) give more details.

Appendix: Ultrashort Laser Pulses and Experimental Techniques

Techniques of femtochemistry involve the use of ultrashort pulses and sensitive methods of detection, and the generation, amplification, and characterization of ultrashort pulses become part of the experiments. The generation of such laser pulses has a rich history, beginning with the realization of the first (ruby) laser in 1960 and the dye laser in 1966. Pulses of picosecond and femtosecond duration are obtained using what is referred to as mode-locking, and in combination with pulse compression methods, a 6-fs pulse was obtained in 1987 from a dye laser at Bell Laboratories, USA. The current state of the art in pulse generation involves self-mode-locking of solid-state lasers (titanium–doped sapphire or Ti:sapphire), which can be operated more routinely and with great reliability; pulses as short as 4 fs have been produced. This self-mode-locking in Ti:sapphire crystal was first observed by researchers at the University of St. Andrews in Scotland. Below, we briefly describe the concepts involved in generation and use of ultrashort pulses, following two recent review articles (*4, 8*).

The laser, light amplification by stimulated emission of radiation, operates on two concepts: amplification and feedback. Thus one must have a gain medium (e.g. Ti:sapphire crystal) for amplification and a cavity (e.g. two mirrors) for the feedback. The excited Ti:sapphire crystal amplifies the light, and with the feedback of the cavity, the bouncing of light back and forth, an intense laser beam is produced from one of the mirrors, which is partially transmitting (Fig. 15). The cavity (of length L) has modes, or light of certain wavelengths, which are separated in frequency by $c/(2L)$. If one mode is isolated, then lasing occurs in a narrow-band frequency in what is referred to as CW or continuous-wave operation. For generation of an ultrashort pulse, light of a large number (possibly millions) of modes (wavelengths) is emitted together coherently; the modes are said to be locked together. Mode-locking is a superposition of light waves in phase (Fig. 15), and as such it is similar to the creation of wave packets of matter waves as described in Section IV. In Figure 15 we also display the shape of a femtosecond pulse at 800 nm; the variation of the electric field at a point may be expressed as

$$E(t) = E_0 \exp\left(-\frac{t^2}{2\sigma^2}\right) \mathrm{Re}\left[\exp(i\omega_0 t)\right] \qquad \text{(A1)}$$

a packet with a carrier frequency $\omega_0/2\pi$ and rms width σ of the field amplitude envelope.

Three essential elements are contained in the cavity of a femtosecond laser: a gain medium, a mode-locking element, and an element that compensates for group velocity dispersion. The gain medium has a broad spectrum to ensure a large number of modes sufficient for femtosecond pulse generation; a 10-fs pulse requires a spectral width of about 100 nm at an 800-nm center wavelength. The group-velocity-disper-

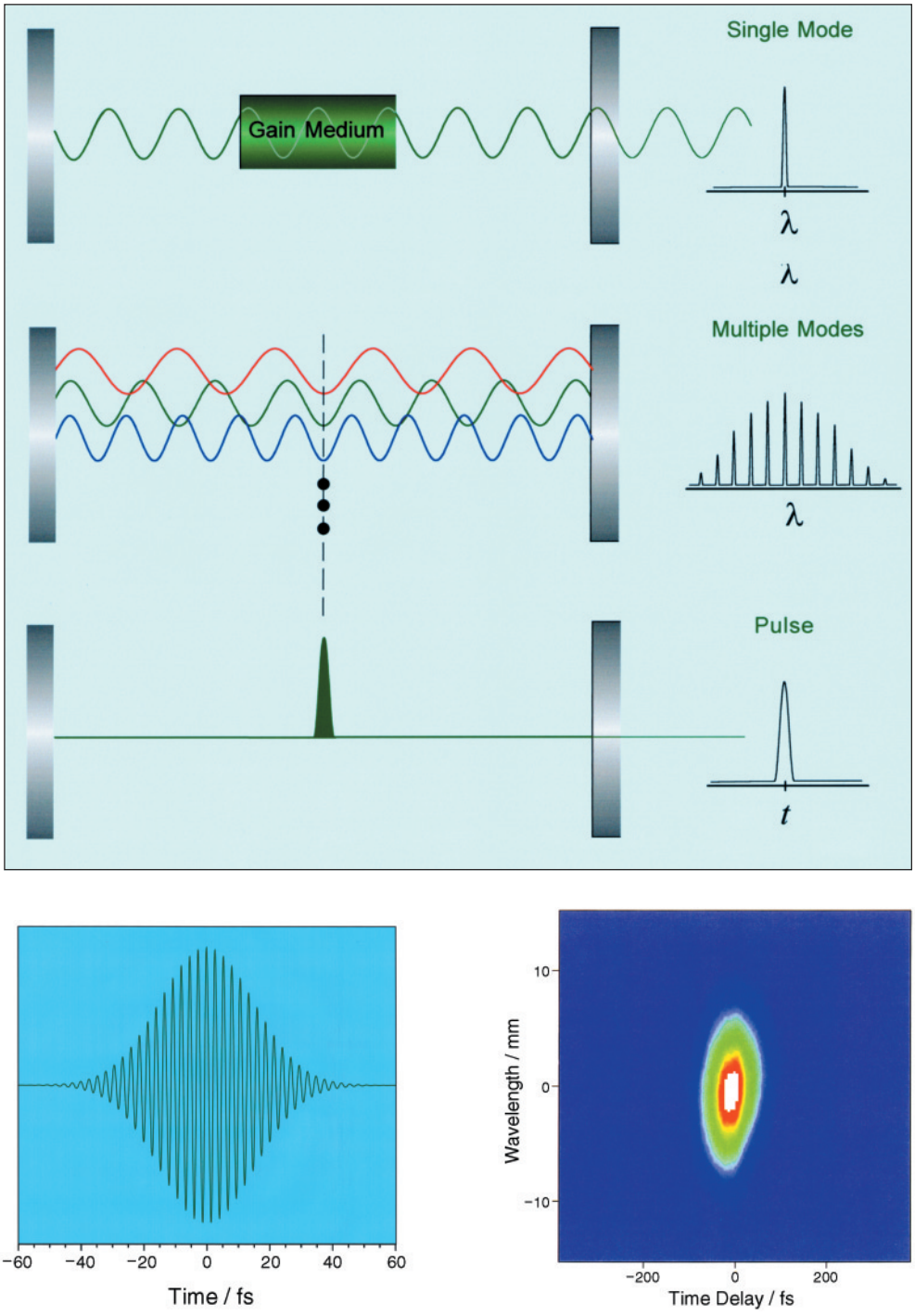

Figure 15. The basic concept of ultrashort-laser-pulse generation by the process of mode-locking.

The upper figure shows (top) continuous-wave lasing in single-mode operation; (middle) the superposition of several modes, which, if locked together in large numbers as indicated by the three vertical dots, gives (bottom) pulsed operation such as that depicted here. Note the analogy with matter's waves superposition in Figure 7.

The lower figures show (left) field of a femtosecond pulse at 800 nm (eq A1, σ = 15 fs), together with (right) an experimental display of a pulse in wavelength (nm)–time (fs) domain.

sion element usually consists of a combination of prisms arranged so that the broad range of spectral components in the pulse can all stay in step while circulating in the cavity. There are two forms of mode-locking, active and passive; the idea is to provide a time-dependent modulation of loss and (or) gain in the cavity. Active mode-locking uses an externally driven modulator, whereas in passive mode-locking an element that lets the pulse itself vary the gain/loss is included in the cavity. One method of passive mode-locking uses an organic molecule as a "saturable absorber" to enhance the propagation of a pulse over that of continuous lasing in the cavity. When the light is so intense that the saturable absorber's rate of absorption exceeds its rate of ground-state population recovery, it becomes temporarily transparent—it is saturated. This transparency occurs at the peak intensity levels of pulsed operation, allowing light to pass and circulate in the cavity to ultimately produce ultrashort pulses; the lower light intensities achievable in continuous lasing are blocked.

For Ti:sapphire lasers, the favoring of pulsed operation is achieved using self-mode-locking. The lasing material has a refractive index that changes depending on the light intensity. Because the laser beam in the cavity has a transverse spatial distribution with the largest intensity in the middle (Gaussian profile), the speed of light propagation for the intense part decreases relative to that of the lower intensity part, resulting in a lens-type focusing behavior (optical Kerr effect). This effect is pronounced only under the high intensities possible with short pulses. With a narrow aperture in the cavity where the pulsed beam focuses, much of the beam from any lower intensity mode of operation, which does not focus, can be blocked, while the pulses pass unimpeded. Thus the favored pulsed lasing will be the natural mode of operation.

To carry out femtosecond experiments, we need both a pump and a probe pulse as discussed in Section IIC. These are usually created from the output of a single femtosecond laser by a variety of nonlinear optical mixing processes chosen to produce the specific wavelengths of light appropriate for the molecule under study. The generated femtosecond pump and probe pulses are characterized by measuring the intensity, duration, spectral bandwidth, and polarization of the fields. The pump pulse sets the $t = 0$ by initiating the molecular process under study, and the relative timing of pump and probe passage through the sample is controlled by an optical delay. The probe pulse is usually absorbed, and the absorption varies as a function of the probe delay time, in response to the spectral changes of atoms or molecules as the reaction proceeds. The amount of probe absorption is reflected in a signal acquired by one of a variety of detection schemes. Two of these are laser-induced fluorescence and mass spectrometry.

In laser-induced fluorescence, the absorption of probe light energy creates an electronically excited species, which then emits light characteristic of the species; that is, it fluoresces. The fluorescence intensity is measured at each delay time to determine the amount of absorption. For example, for NaI (discussed in Section IVD), the absorption spectra of various configurations of the transition-state complex Na···I are very different from those of free Na and I atoms. Thus by tuning the probe to the wavelength absorbed by Na···I with Na and I close together we can observe a periodic fall and rise of the fluorescence signal with delay as the population vibrates back and forth in the quasi-bound well, passing repeatedly through the strongly absorbing configuration (Fig. 9). Since some of the molecules break apart with every bounce, the peak of every return is also smaller than the last. On the other hand, when the probe is tuned to a wavelength absorbed by free Na atoms, the fluorescence increases in stepwise fashion (Fig. 9) as, at each bounce, a new batch of free atoms is added to the existing pool; for the entire process all molecules move coherently.

In mass spectrometric detection, the probe creates a population of ions which can be sorted by mass. Thus, changes in mass as well as changes in absorption spectra can be monitored as bonds are broken and formed. There are variant methods of detection such as photoelectron spectroscopy (*4*). Ultrafast electron diffraction is being developed to observe the bond length change with time for more complex structures (*7*).